Supporting Information

Rational design of ultrathin 2D tin nickel selenide nanosheets for high-performance flexible supercapacitors

Thangasamy Deepalakshmi,[a] Thanh Tuan Nguyen,[b] Nam Hoon Kim,[b] Kil To Chong [a*] and Joong Hee Lee[b,c*]

[a]Department of Electronics Engineering, Advanced Research Center of Electronics and Information, Jeonbuk National University, Jeonju, Jeonbuk, 54896, Republic of Korea

[b]Advanced Materials Institute of BIN Convergence Technology (BK21 Plus Global) & Dept. of BIN Convergence Technology, Jeonbuk National University, Jeonju, Jeonbuk, 54896, Republic of Korea

[c]Carbon Composite Research Centre, Department of Polymer - Nano Science and Technology, Jeonbuk National University, Jeonju, Jeonbuk, 54896, Republic of Korea

---

Corresponding author: Fax: +82 63 270 2341; Tel: +82 63 270 2342

Email address: Email: kitchong@jbnu.ac.kr (Prof. Kil To Chong)
Email: jhl@jbnu.ac.kr (Prof. Joong Hee Lee)

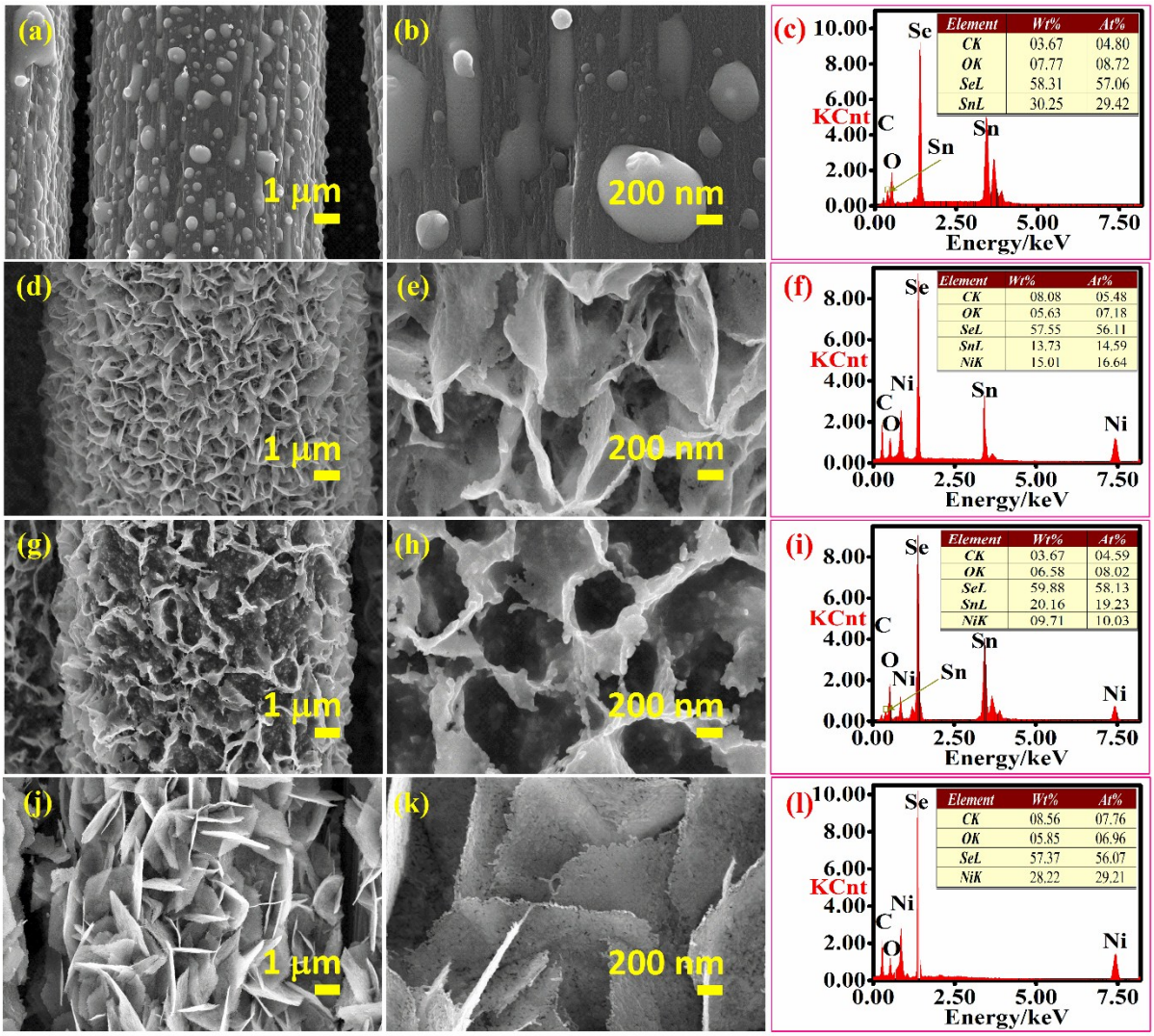

Fig. S1 SEM and high-resolution SEM images of (a, b) $SnSe_2$, (d, e) $Sn_{0.5}Ni_{0.5}Se_2$, (g, h) $Sn_{0.67}Ni_{0.33}Se_2$, and (j, k) $NiSe_2$ nanostructures. EDX spectra of (c) $SnSe_2$, (f) $Sn_{0.5}Ni_{0.5}Se_2$, (i) $Sn_{0.67}Ni_{0.33}Se_2$, and (l) $NiSe_2$ nanostructures.

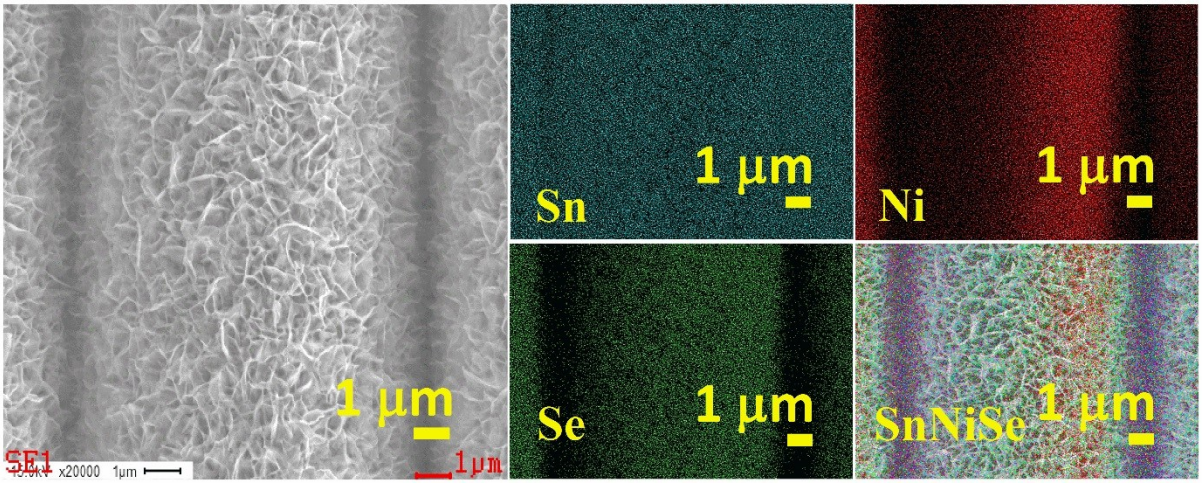

Fig. S2 SEM-EDS color elemental mapping of $Sn_{0.33}Ni_{0.67}Se_2$ NAs in terms of Sn-K, Ni-K, and Se-K.

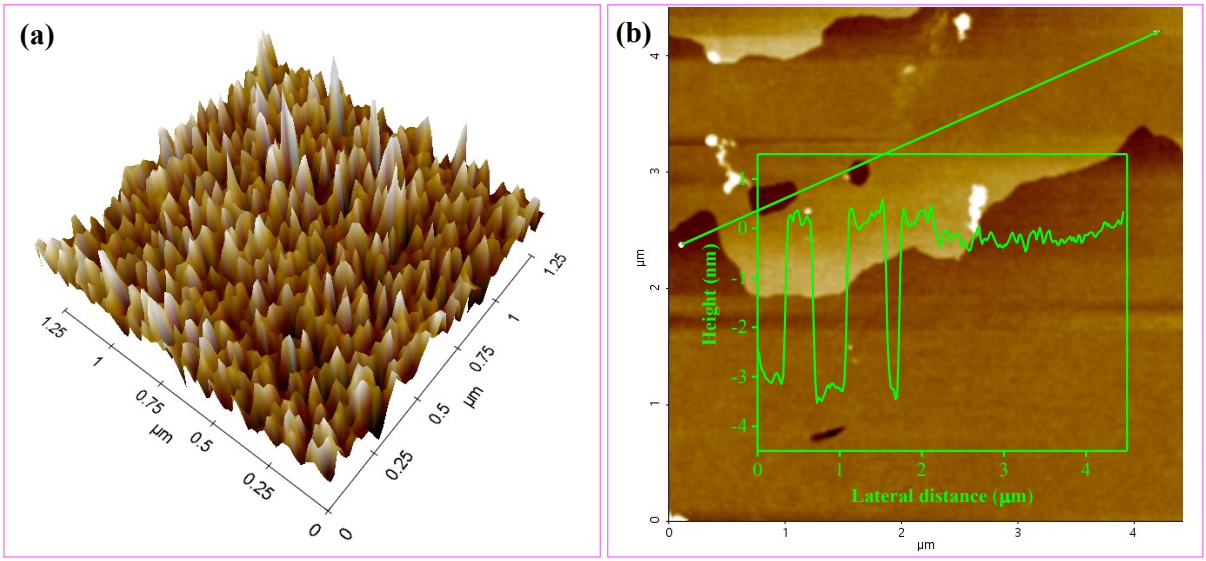

Fig. S3 (a) 3D and (b) 2D AFM images and its height profile of $Sn_{0.33}Ni_{0.67}Se_2$ representing the thickness of few nanometer and width > 4 µm.

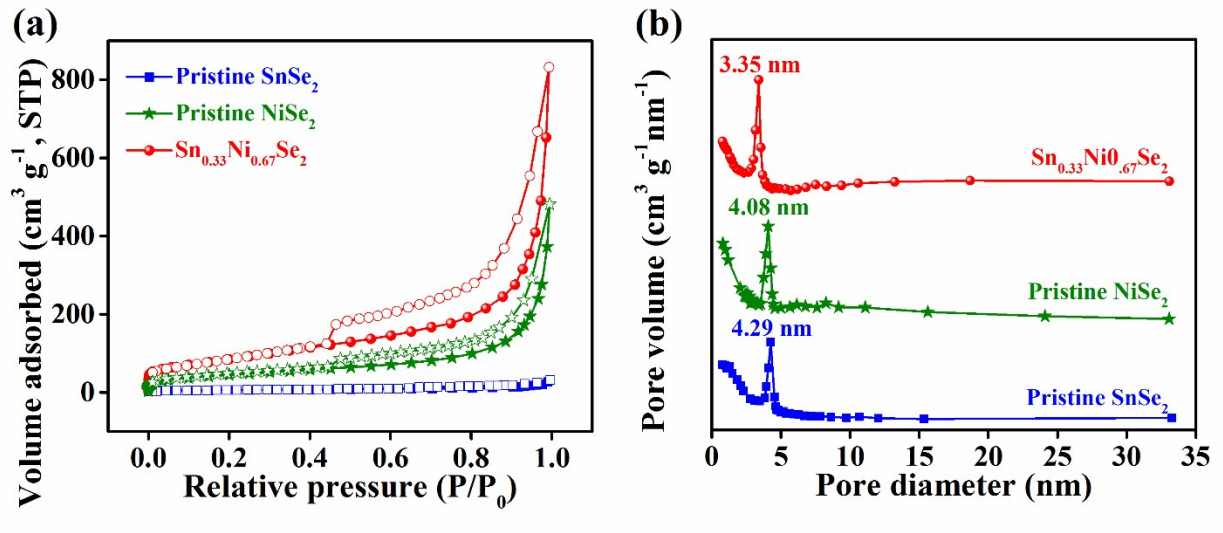

Fig. S4 (a) N_2 adsorption-desorption isotherms and (b) their corresponding pore size distribution of pristine $SnSe_2$, $NiSe_2$, and $Sn_{0.33}Ni_{0.67}Se_2$ NAs.

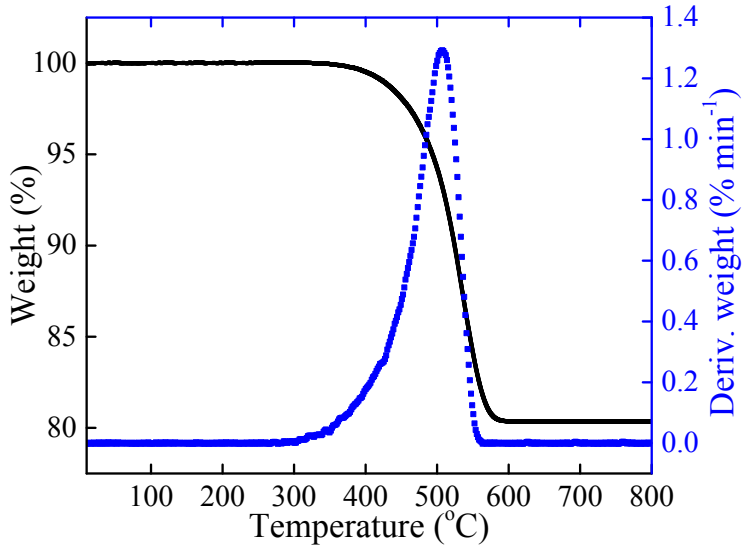

Fig. S5 TGA curves of $Sn_{0.33}Ni_{0.67}Se_2$ NAs under air flow with a temperature ramp of ~5 °C min^{-1}.

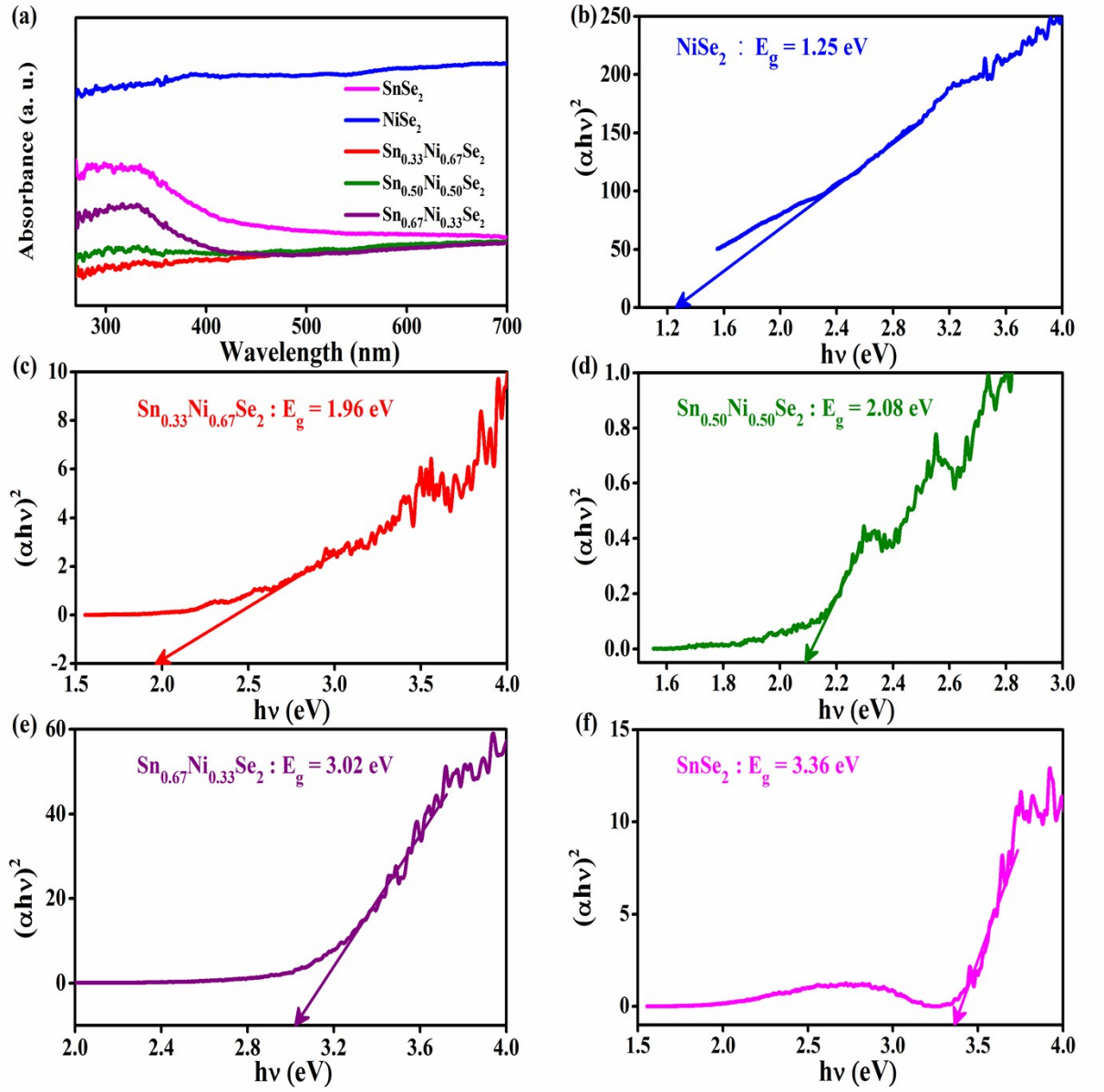

Fig. S6 (a) UV–vis DRS spectra and (b-f) bandgap measurements of $Sn_xNi_{1-x}Se_2$ nanostructures.

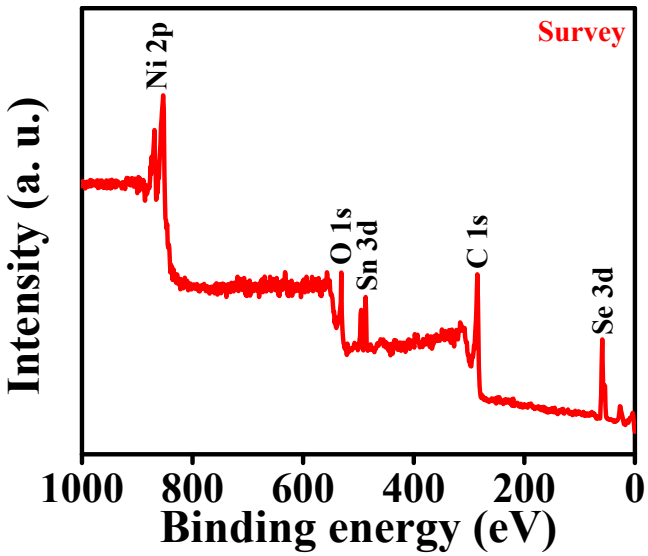

Fig. S7 XPS survey spectrum of $Sn_{0.33}Ni_{0.67}Se_2$ NAs.

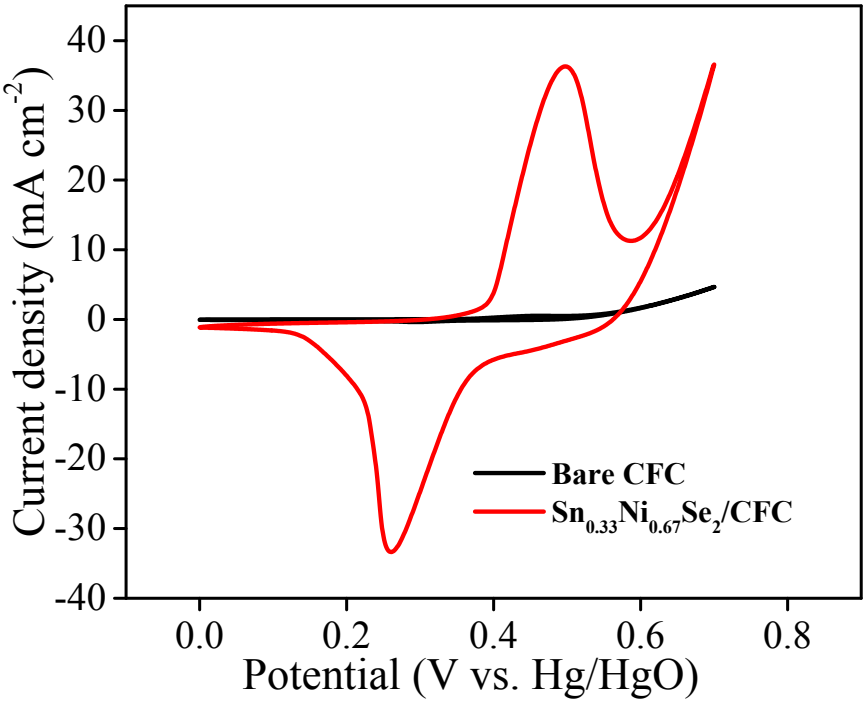

Fig. S8 CV curves of bare CFC and $Sn_{0.33}Ni_{0.67}Se_2$ NAs/CFC electrode at a scan rate of 50 mV s^{-1}.

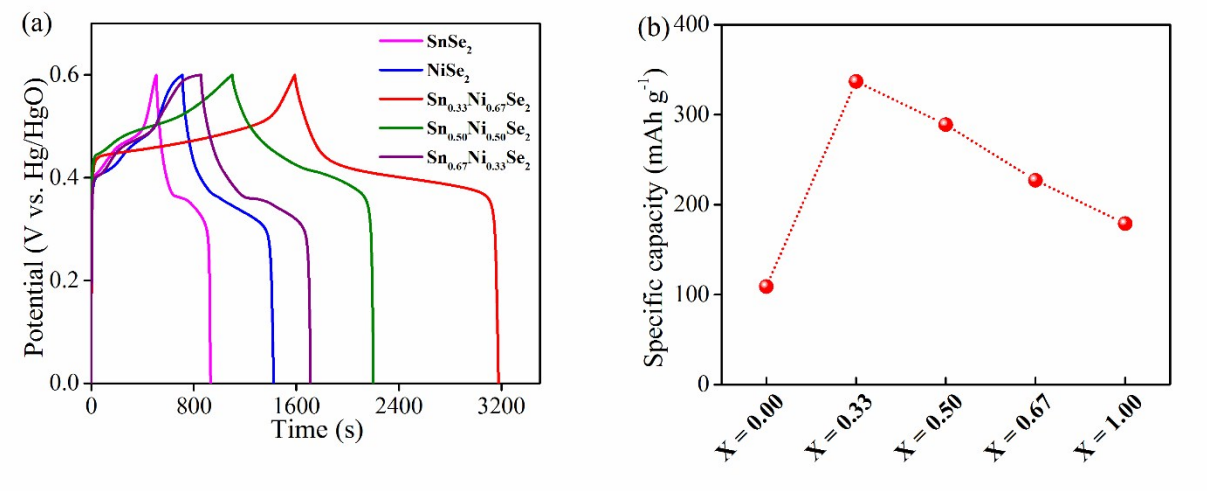

Fig. S9 (a) GCD curves of $Sn_xNi_{1-x}Se_2$ electrodes with different *x* values using there-electrode system at a current density of 1 mA cm^{-2} and (b) specific capacity values calculated from GCD data at different *x* values.

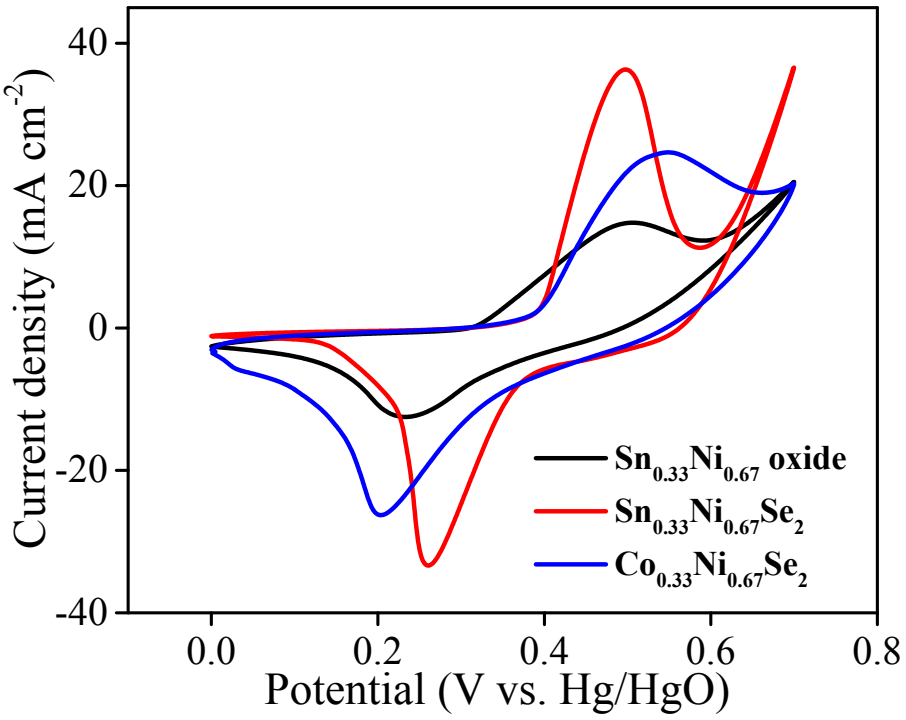

Fig. S10 Comparisons between the $Sn_{0.33}Ni_{0.67}Se_2$ electrode, $Co_{0.33}Ni_{0.67}Se_2$ electrode, and $Sn_{0.33}Ni_{0.67}$ oxide electrode perceived from heat treatment of their corresponding LDH precursors at 350 °C at air atmosphere: CVs measured at a high scan rate of 50 mV s^{-1}.

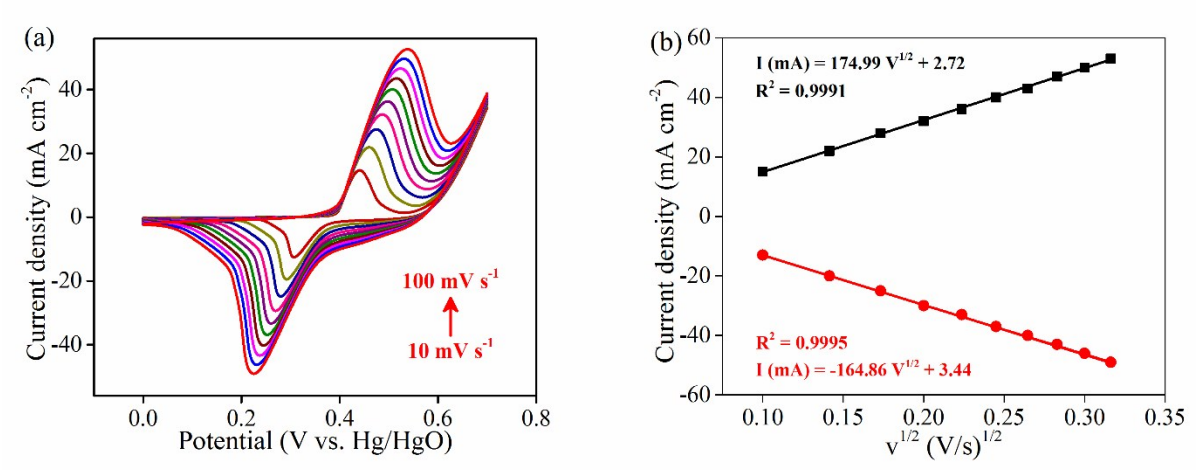

Fig. S11 (a) CV curves of $Sn_{0.33}Ni_{0.67}Se_2$ electrode with different scan rates from 10 to 100 mV s^{-1} and (b) the relationship of redox peak current *vs.* square root of scan rate.

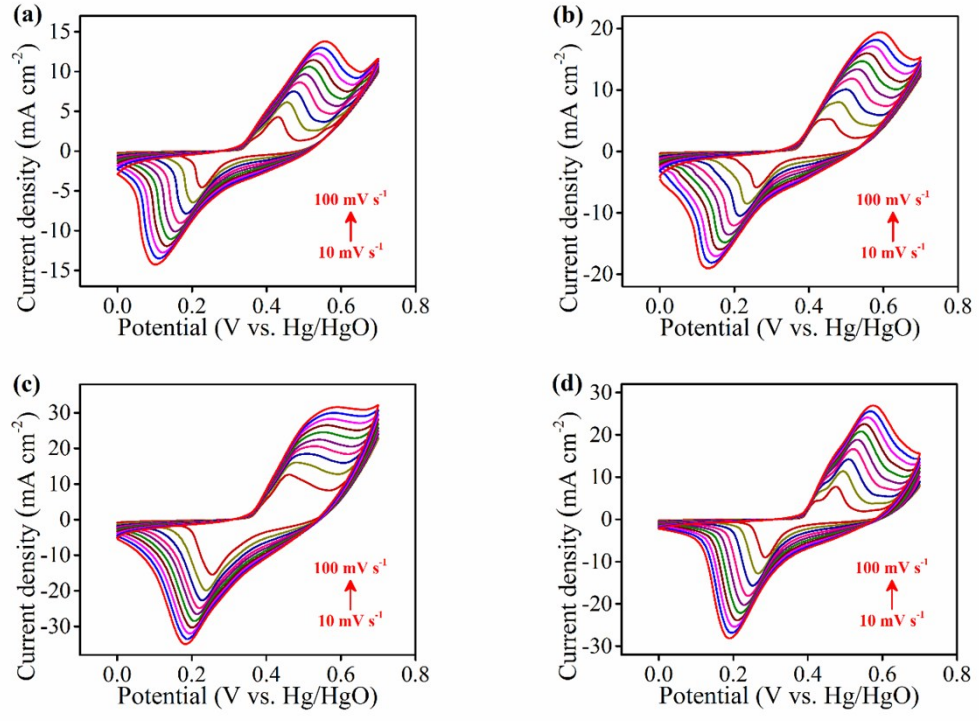

Fig. S12 CV curves with different scan rates from 10 to 100 mV s^{-1} of (a) $SnSe_2$, (b) $NiSe_2$, (c) $Sn_{0.5}Ni_{0.5}Se_2$, and (d) $Sn_{0.67}Ni_{0.33}Se_2$ electrodes.

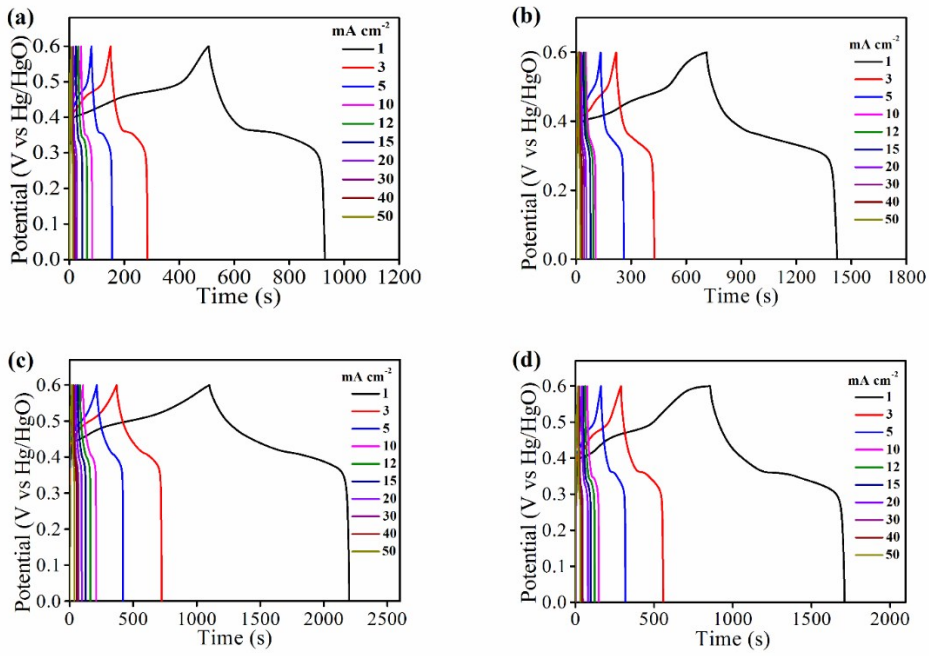

Fig. S13 GCD curves with various 1 to 50 mA cm^{-2} of (a) $SnSe_2$, (b) $NiSe_2$, (c) $Sn_{0.5}Ni_{0.5}Se_2$, and (d) $Sn_{0.67}Ni_{0.33}Se_2$ electrodes.

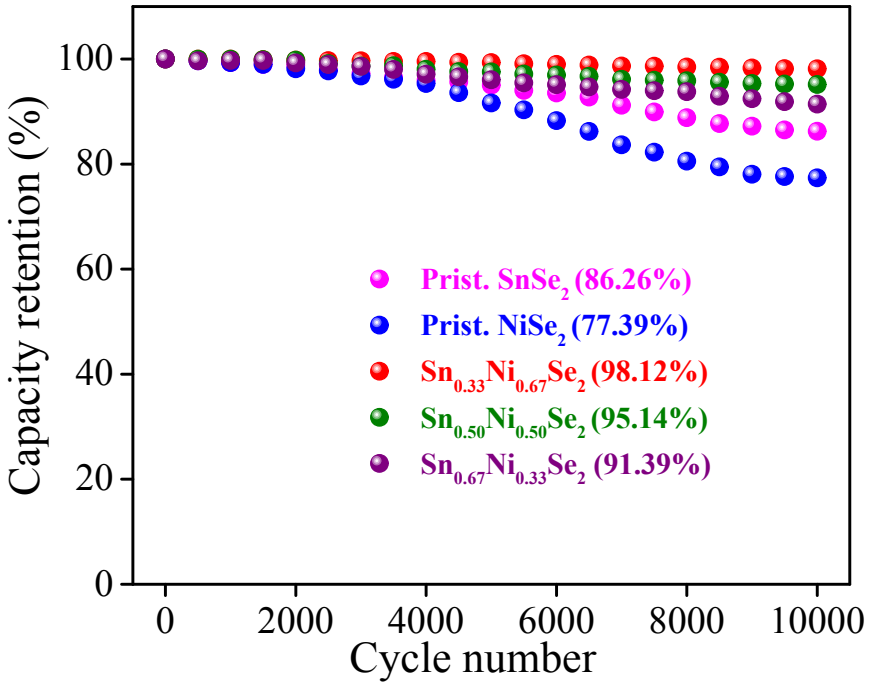

Fig. S14 Cycling performance of $SnSe_2$, $NiSe_2$, $Sn_{0.33}Ni_{0.67}Se_2$, $Sn_{0.5}Ni_{0.5}Se_2$, and $Sn_{0.67}Ni_{0.33}Se_2$ electrodes at a higher current density of 30 mA cm^{-2}.

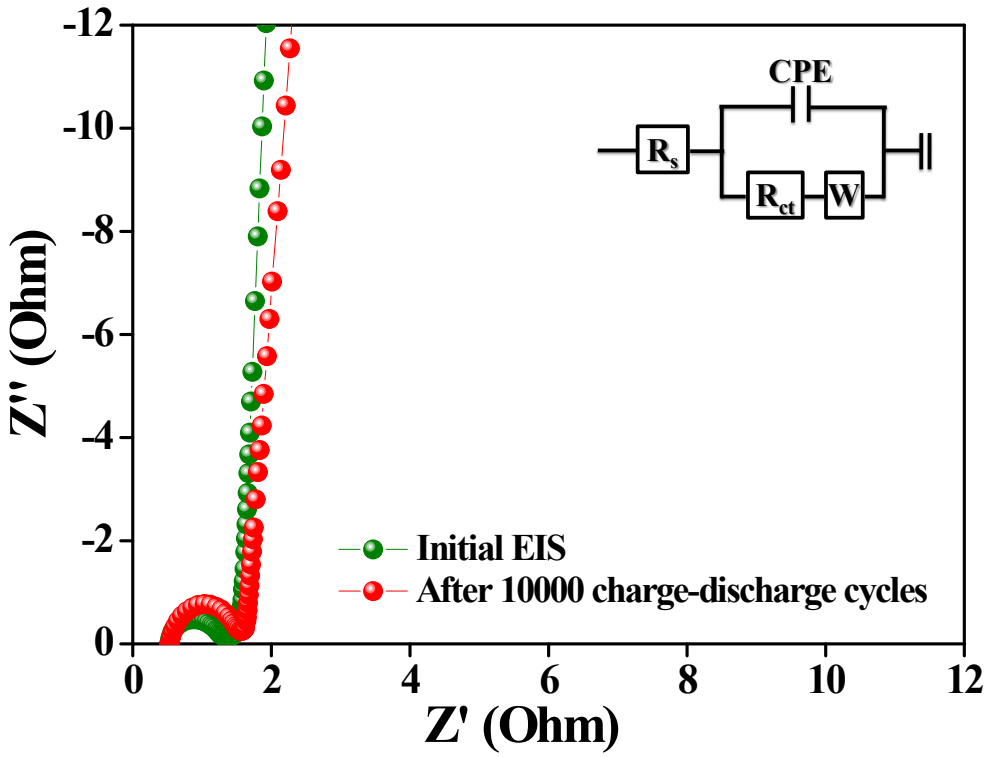

Fig. S15 EIS of optimal $Sn_{0.33}Ni_{0.67}Se_2$ electrode using there-electrode system (initial and after successive 10000 charge–discharge cycles).

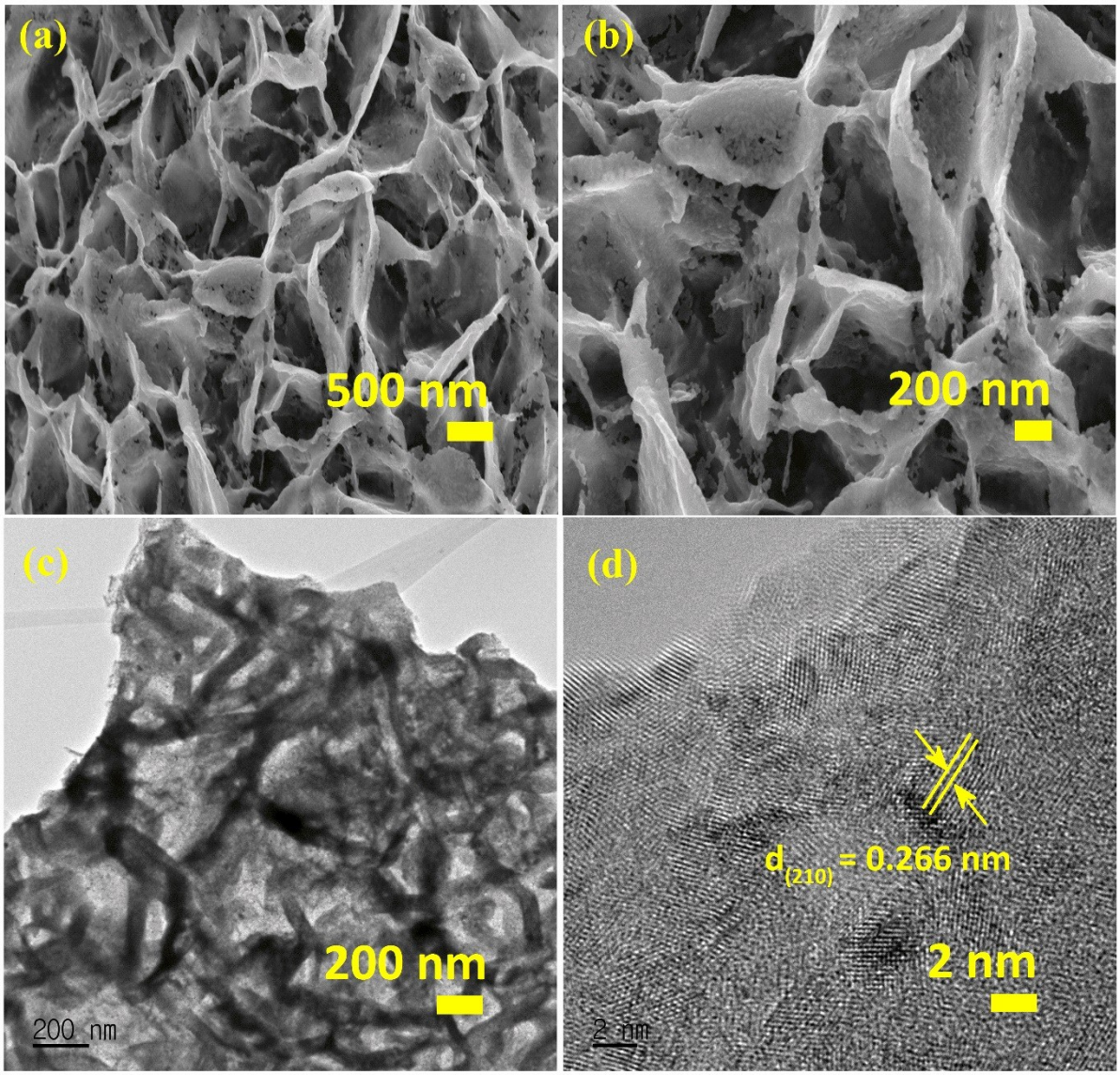

Fig. S16 (a, b) SEM images with different magnifications and (c, d) TEM images with different magnifications of $Sn_{0.33}Ni_{0.67}Se_2$ NAs (after successive 10000 charge–discharge cycles).

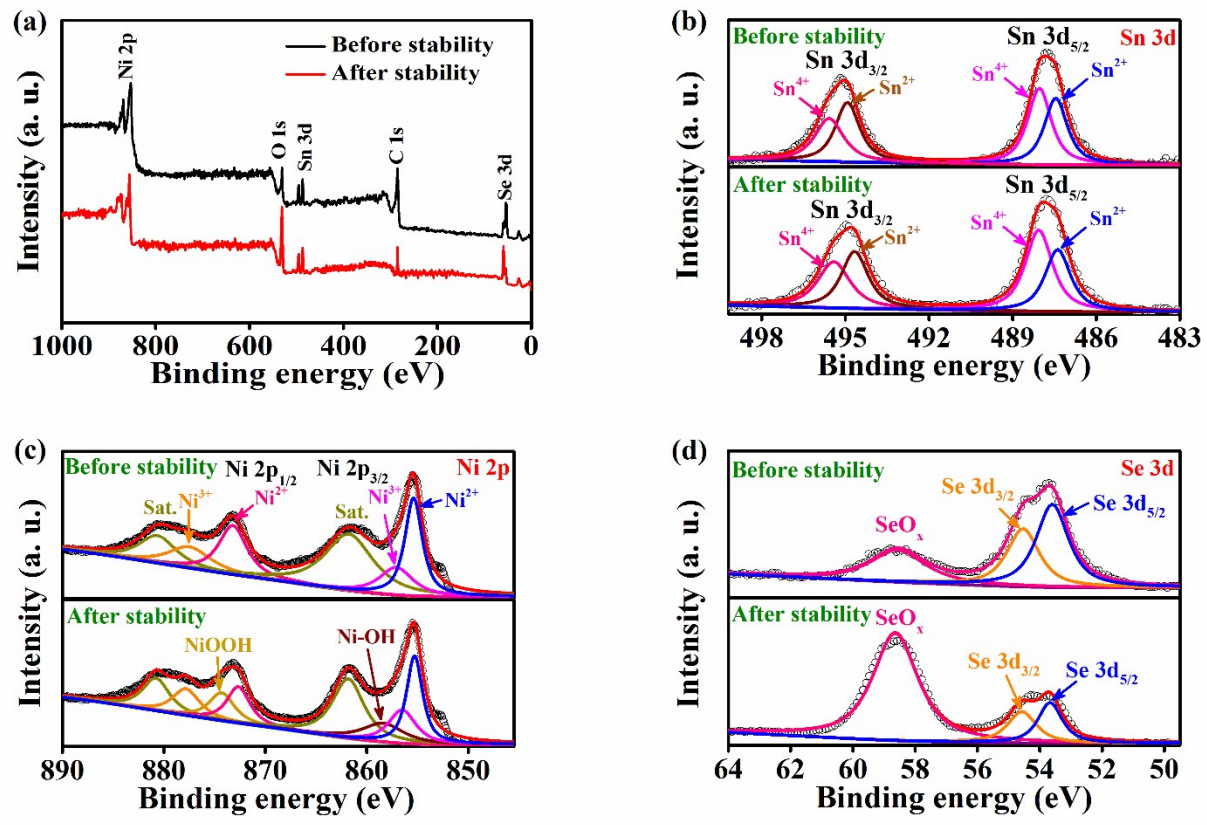

Fig. S17 XPS before and after successive 10000 charge–discharge cycles.

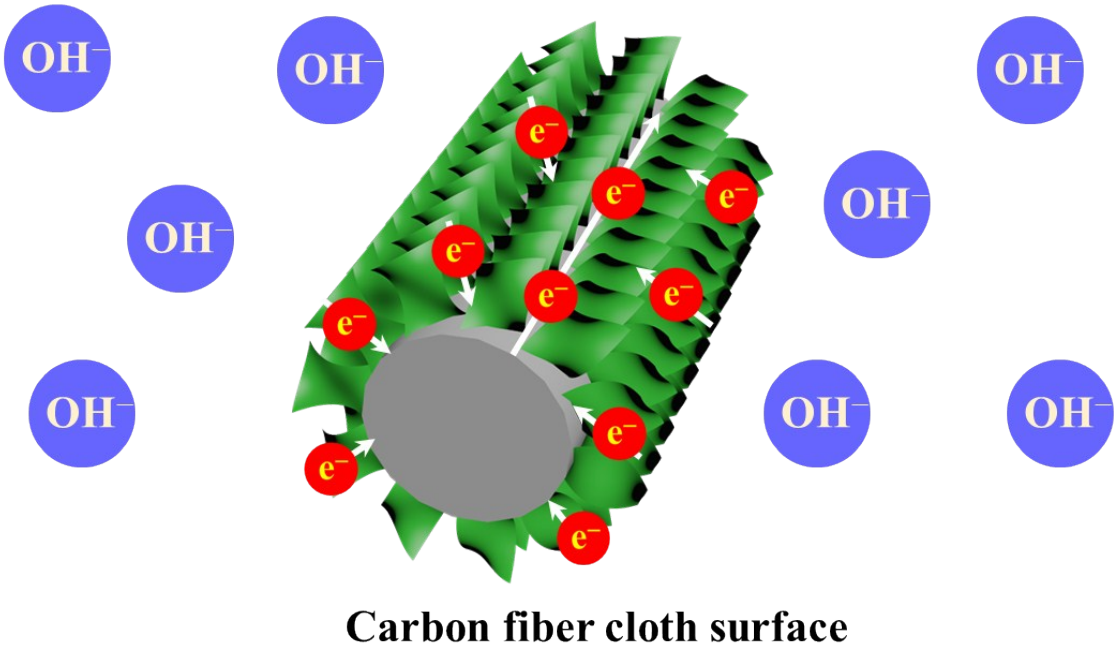

Fig. S18 Schematic diagram of the virtues of the interconnected ultra-thin $Sn_{0.33}Ni_{0.67}Se_2$ NAs.

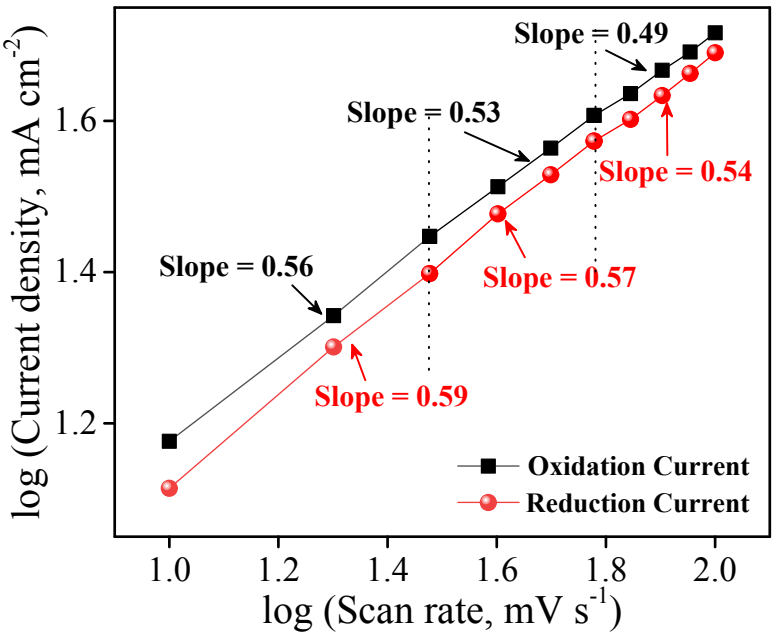

Fig. S19 Calculated *b*-value of the oxidation and reduction peak currents at scan rate of 10 to 100 mV s^{-1} of $Sn_{0.33}Ni_{0.67}Se_2$ electrode.

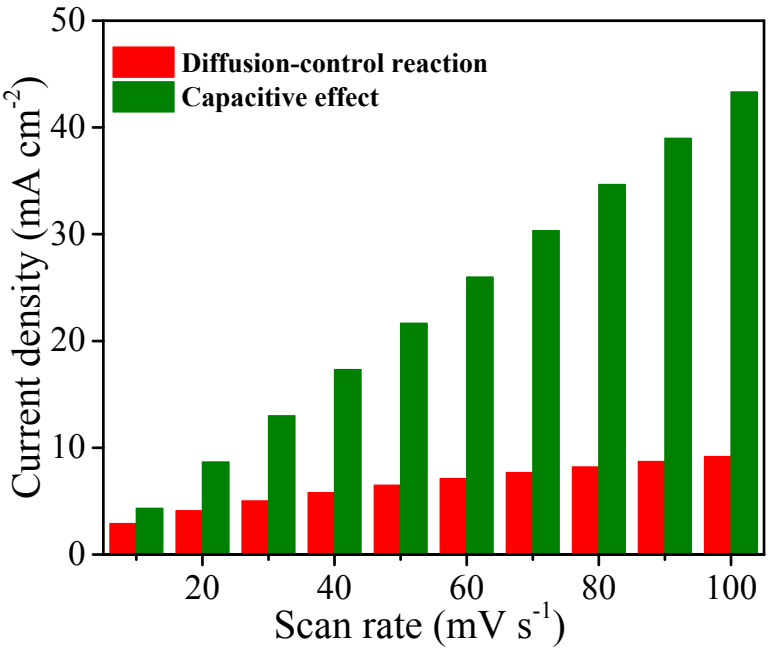

Fig. S20 Calculated surface pseudocapacitive and bulk-insertion typed current density at various scan rates of $Sn_{0.33}Ni_{0.67}Se_2$ electrode.

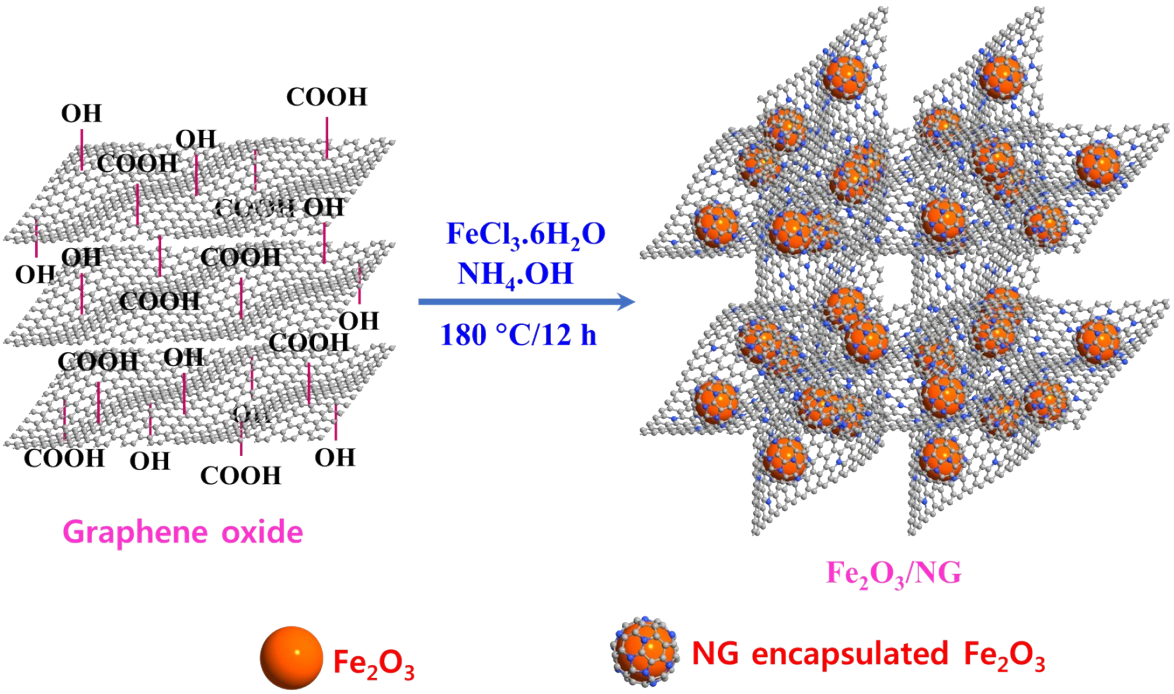

Fig. S21 Schematic illustration for the synthesis of Fe_2O_3@NG hydrogel by in-situ hydrothermal method.

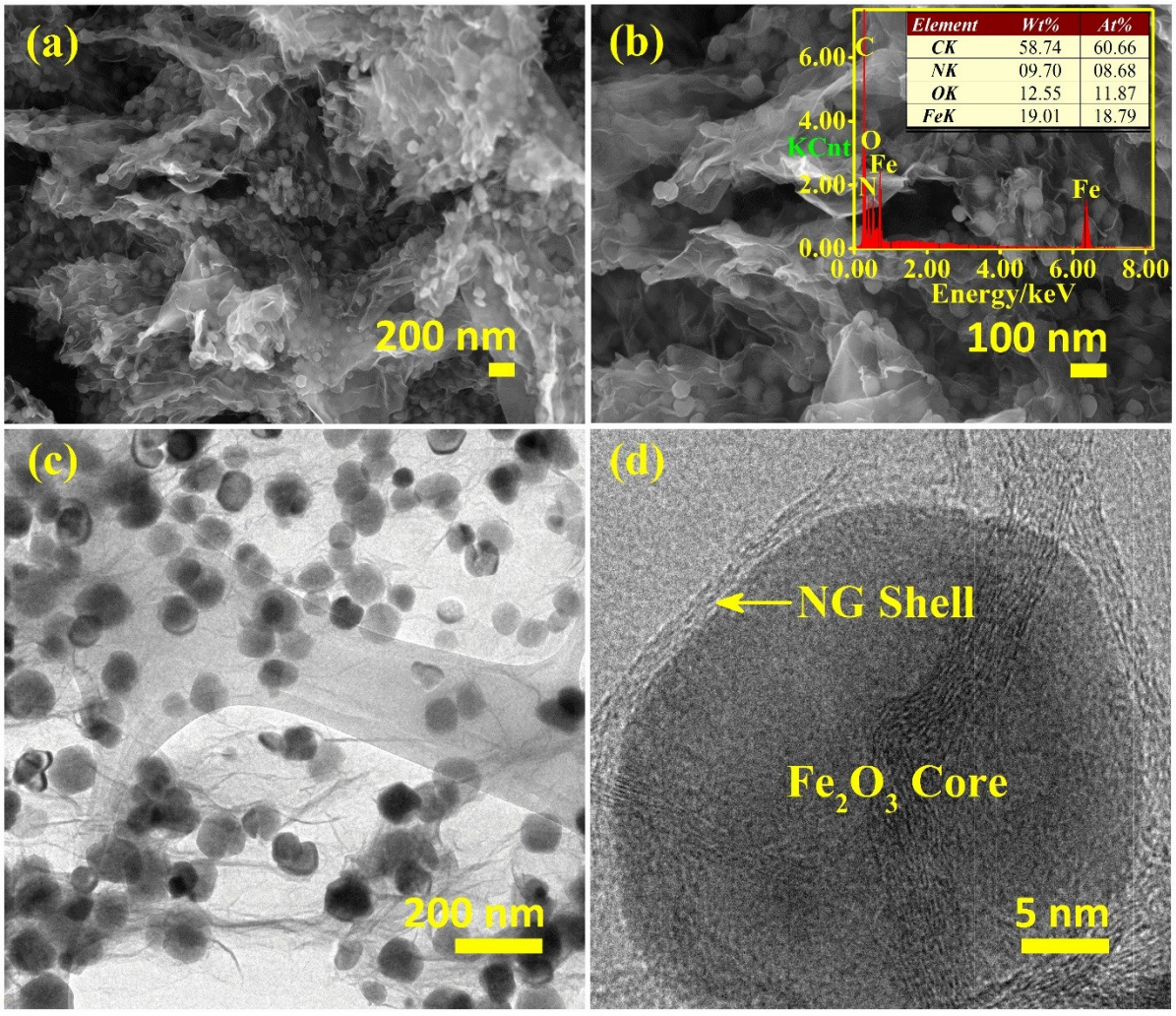

Fig. S22 (a, b) SEM images with different magnifications (inset shows the corresponding EDX analysis), (c) TEM, and (d) HR-TEM images of the as-synthesized Fe_2O_3@NG hydrogel.

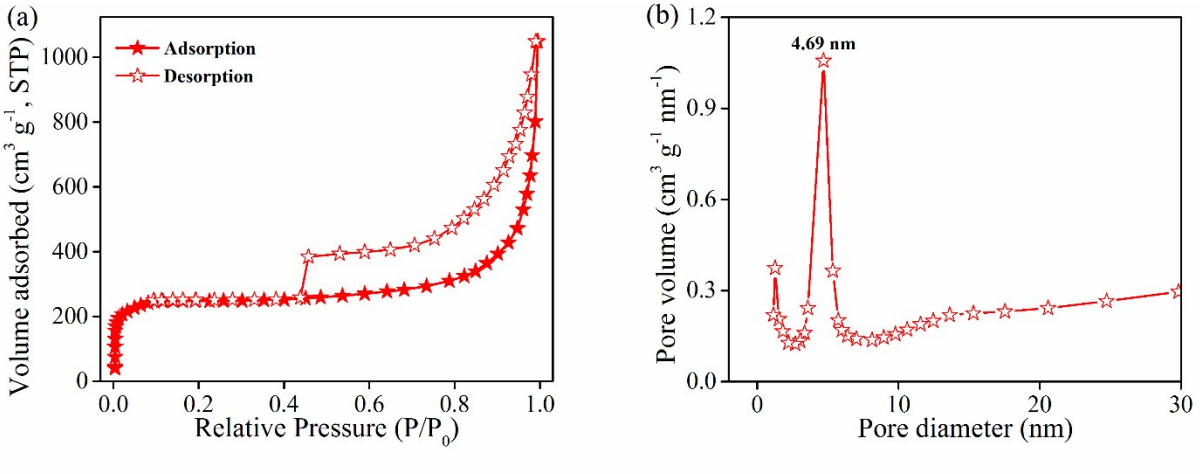

Fig. S23 (a) N_2 adsorption-desorption isotherms and (b) pore size distribution of the as-synthesized Fe_2O_3@NG hydrogel.

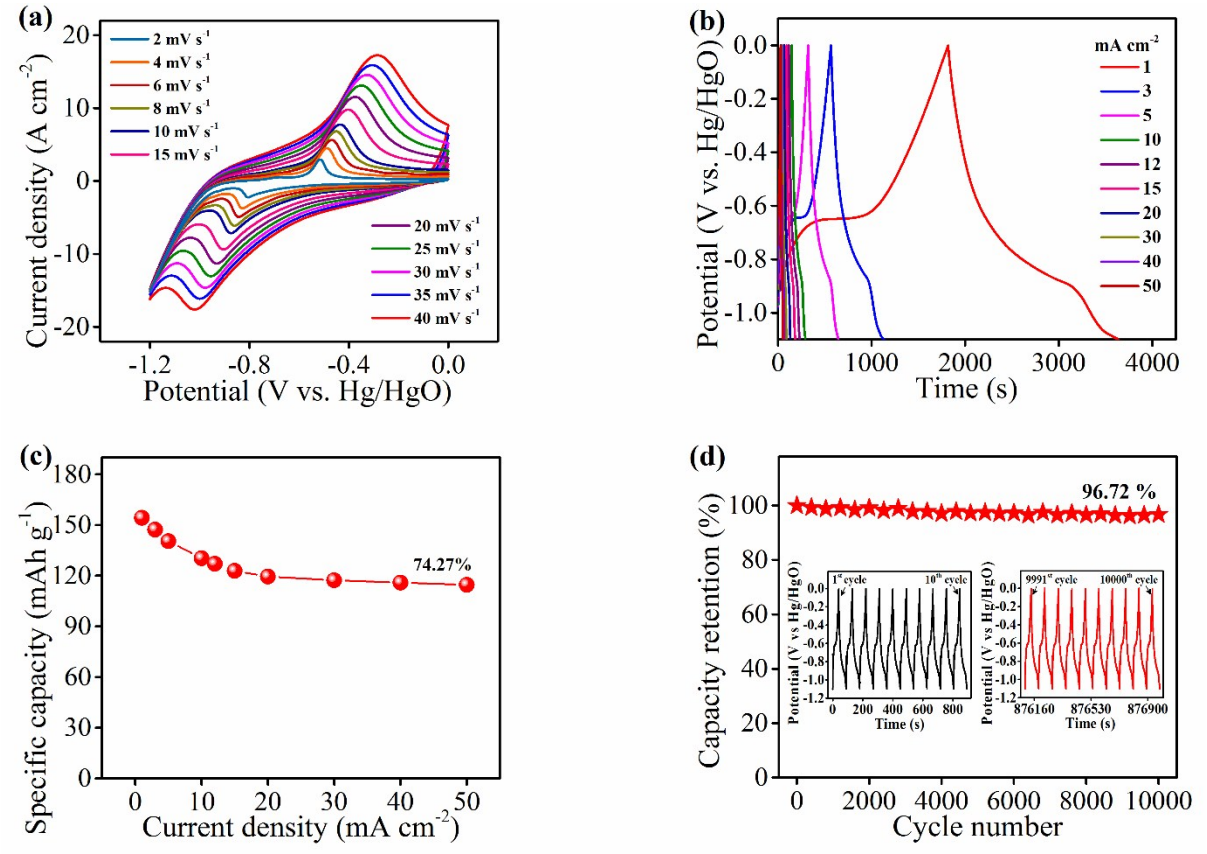

Fig. S24 (a) CV curves of Fe_2O_3@NG hydrogel at different scan rates from 10 to 100 mV s^{-1}, (b) GCD curves of Fe_2O_3@NG hydrogel at various current densities from 1 to 50 A g^{-1}, (c) specific capacity *vs.* current density of Fe_2O_3@NG hydrogel, and (d) Cycling performance of Fe_2O_3@NG hydrogel electrode at a higher current density of 30 A g^{-1} (inset shows the initial and last 10 charge–discharge cycles).

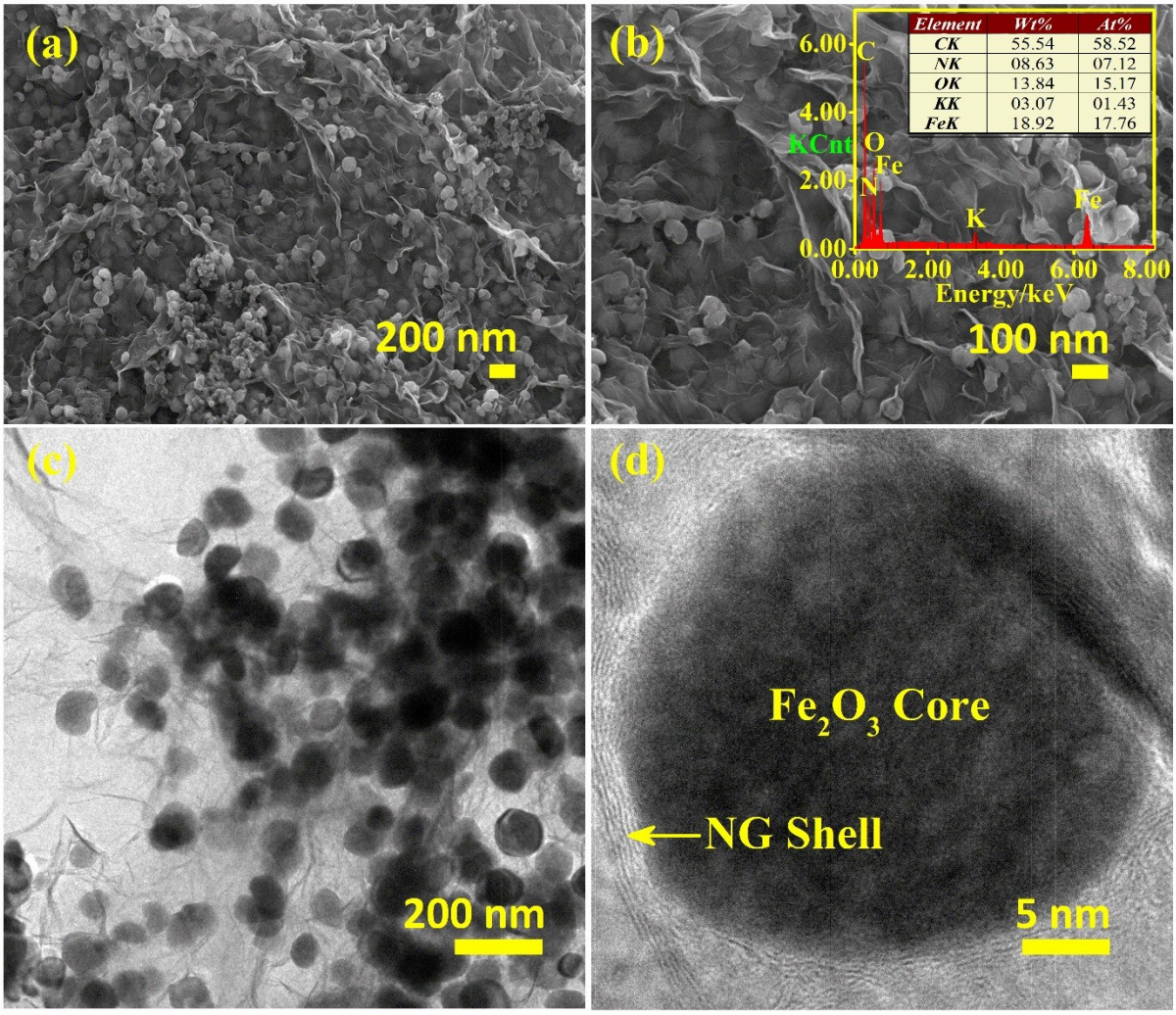

Fig. S25 (a, b) SEM images with different magnifications (inset shows the corresponding EDX analysis), (c) TEM, and (d) HR-TEM images of the as-synthesized Fe_2O_3@NG hydrogel (after successive 10000 charge–discharge cycles).

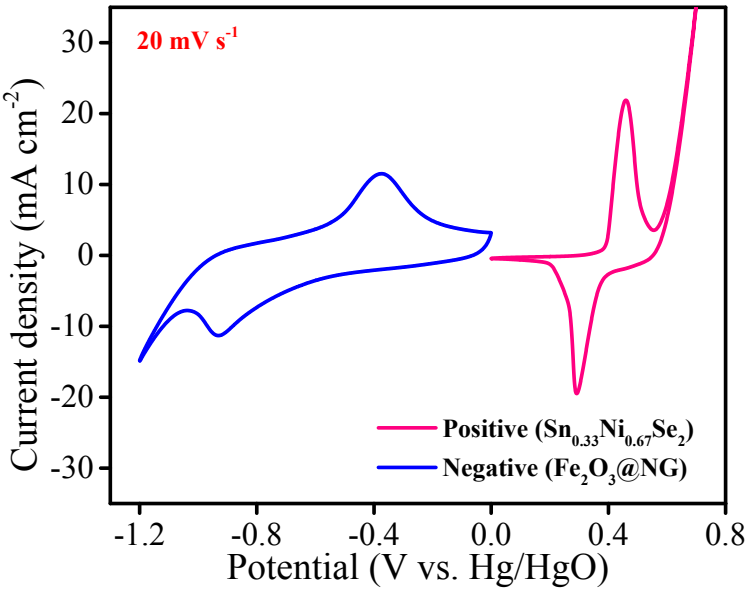

Fig. S26 CV curves of the $Sn_{0.33}Ni_{0.67}Se_2$ and Fe_2O_3@NG electrodes in three-electrode setup at a scan rate of 20 mV s^{-1}.

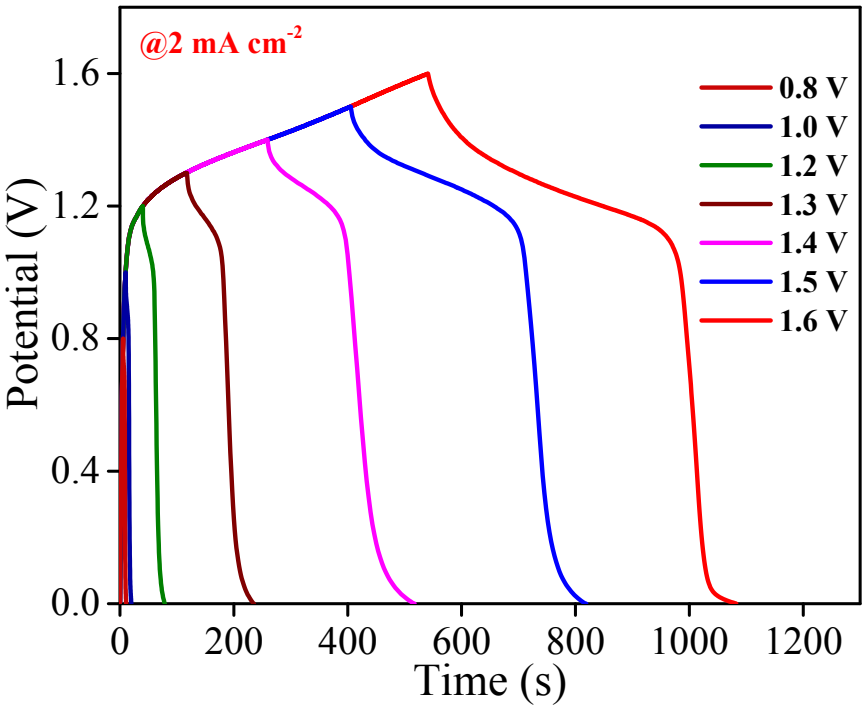

Fig. S27 GCD curves (at a current density of 2 mA cm^{-2}) of the flexible solid-state ASC collected at different potential windows from 0.8 to 1.6 V.

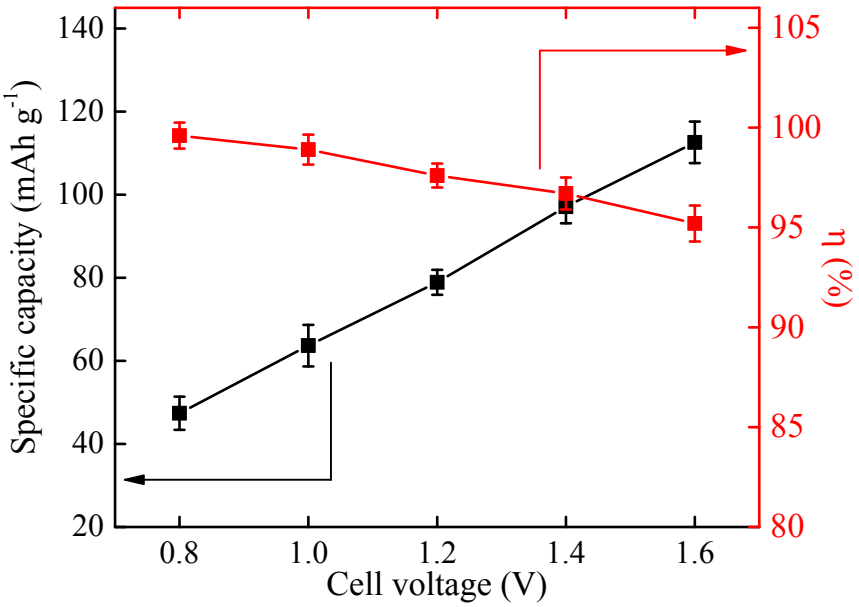

Fig. S28 Coulombic efficiency and specific capacity of flexible solid-state ASC in gel PVA-KOH electrolyte *vs.* different cell voltage.

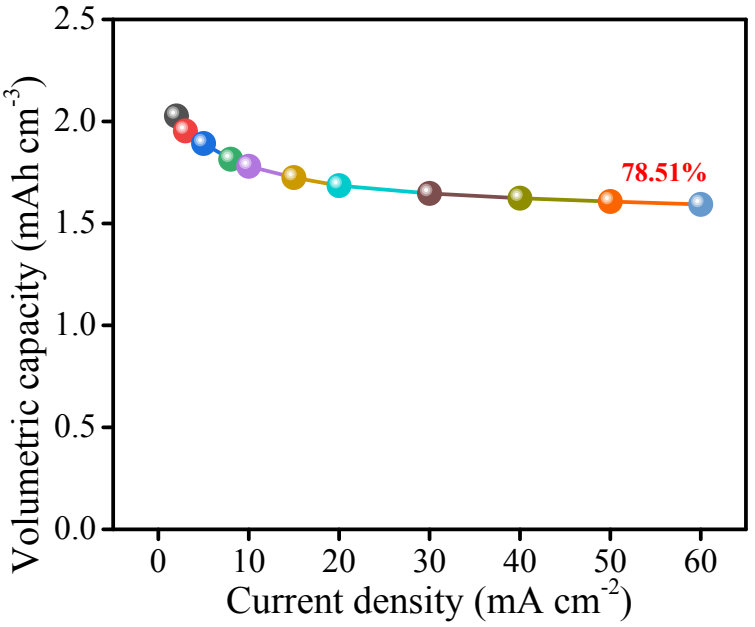

Fig. S29 Volumetric capacity of flexible solid-state ASC at various current densities from 2 to 60 mA cm^{-2}.

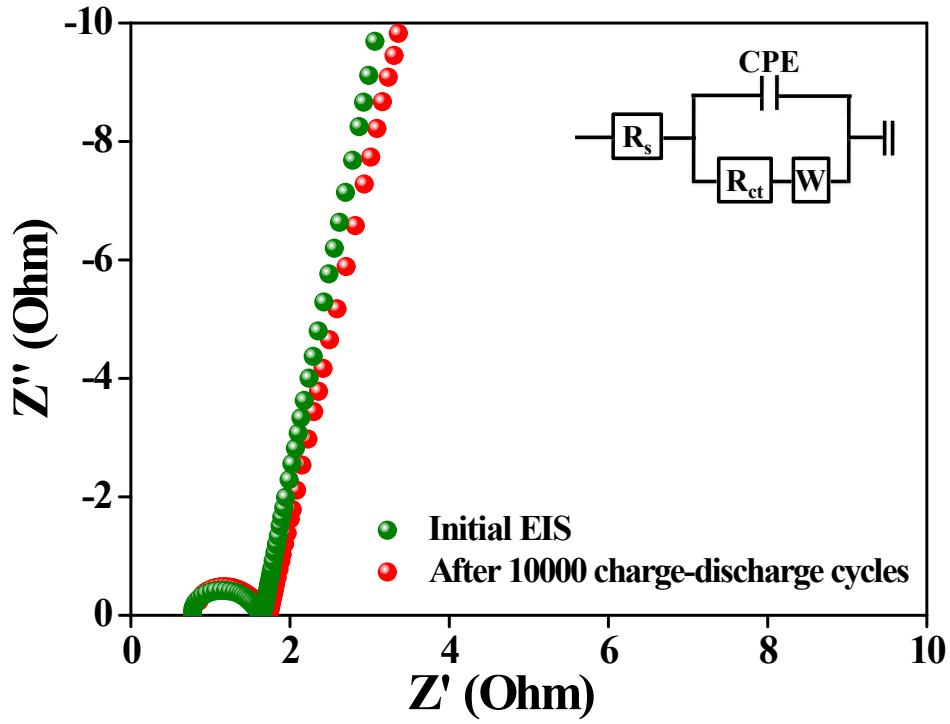

Fig. S30 EIS of optimal flexible solid-state ASC device (initial and after successive 10000 charge–discharge cycles).

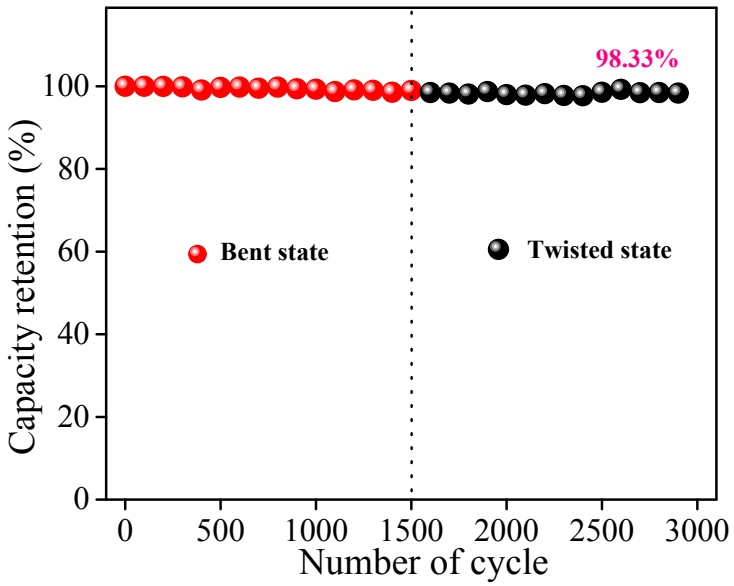

Fig. S31 (a) CV curves of flexible solid-state ASC at normal, different twisting and bent state, and (b) Durability of the flexible solid-state ASC when tested under bending and twisting states. The flexible solid-state ASC retain ~98.33% of its initial capacity after successive 1500 cycles under the bent state, surveyed by another successive 1500 cycles under the twisted state.

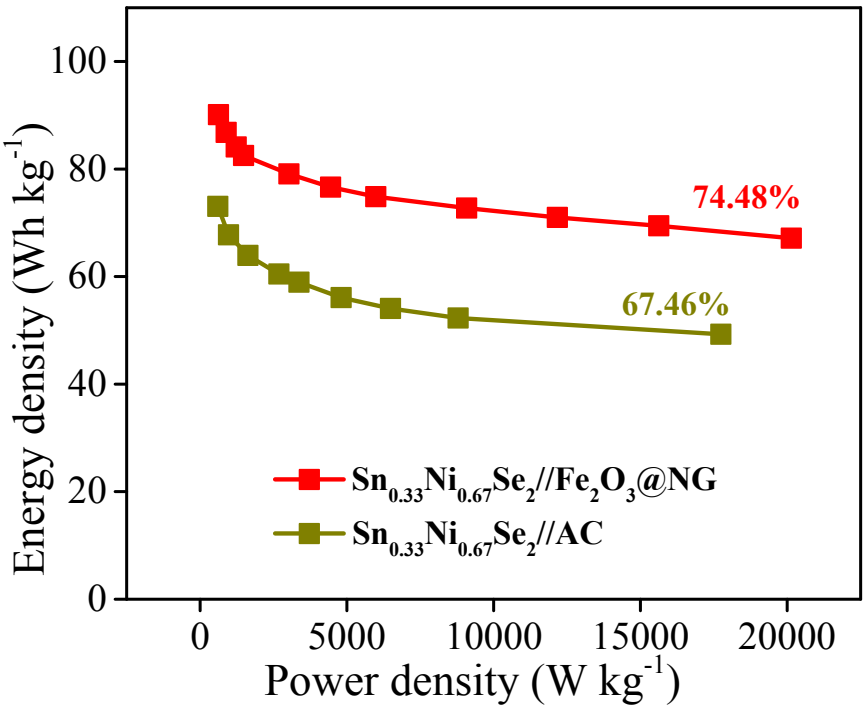

Fig. S32 Ragone plot (specific energy density *vs.* specific power density) of flexible solid-state ASC.

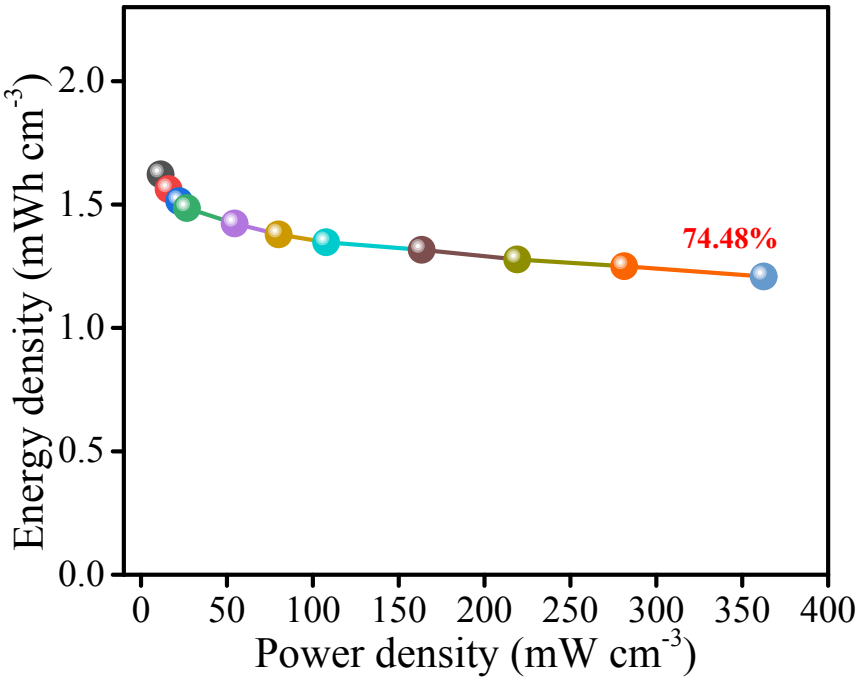

Fig. S33 Volumetric energy density *vs.* volumetric power density of flexible solid-state ASC.

Table S1. Elemental composition of $Sn_xNi_{1-x}Se_2$ nanostructures with different *x* values estimated from ICP-OES.

Samples	**Sn (at. %)**	**Ni (at. %)**	**Se (at. %)**	**O (at. %)**	**C (at. %)**
$SnSe_2$	28.46		57.62	7.14	6.78
$NiSe_2$		28.29	58.67	6.82	6.22
$Sn_{0.33}Ni_{0.67}Se_2$	9.49	19.35	57.03	6.95	7.18
$Sn_{0.5}Ni_{0.5}Se_2$	14.77	15.13	56.32	6.72	7.06
$Sn_{0.67}Ni_{0.33}Se_2$	19.41	10.17	56.56	7.01	6.85

Sn, Ni, Se, O and C contents were detected by ICP-OES measurement.

Table S2. Flexible ASC device properties comparison with the reported literature.

Reported Devices	Electrolyte	Device window (V)	Energy density (W h kg^{-1})	Power density (W kg^{-1})	Stability (Cycles)	Reference
$Sn_{0.33}Ni_{0.67}Se_2$//Fe_2O_3@NG	KOH-PVA	0-1.6 V	90.3	631	96.41% (10000 cycles)	This work
Ni_3Se_2 NSs@CF//AC@CC	1 M KOH + 0.02 m $K_3Fe(CN)_6$	0-1.5 V	32.8	677	98% (5000 cycles)	1
AC//H-$NiCoSe_2$	6 M KOH	0-1.5 V	25.5	3750	82.3% (5200 cycles)	2
$(Ni_{0.1}Co_{0.9})_9Se_8$@NF//rGO@NF	PVA/KOH	0-1.6 V	17.0	3100	88.8% (3000 cycles)	3
Graphene//$(NiCo)_{0.85}Se$	1 M KOH	0-1.8 V	12.5	112.5	85% (10 000 cycles)	4
CC/H-Ni@Al-Co-S//multilayer graphene/CNT	PVA-KOH	0-1.8 V	65.7	765.3	90.6% (10 000 cycles)	5
$NiCo_2S_4$//CFP-AC	2 M KOH	0-1.5 V	180	17.3	88.6% (5 000 cycles)	6
Ni-Co-S/G//PCNS	6 M KOH	0-1.6 V	43.3	800	85% (10 000 cycles)	7
$NiCo_2S_4$//G/CS	6 M KOH	0-1.6 V	42.3	476	78.6% (10 000 cycles)	8
$NiCo_2S_4$/NCF//OMC/NCF	6 M KOH	0-1.6 V	45.5	512	70.4% (10 000 cycles)	9
Ni_3Se_2@$Ni(OH)_2$//AC	7 M KOH	0-1.6 V	50.9 Wh L^{-1}	83.62 W L^{-1}	83.6% (10 000 cycles)	10
$Ni_{0.67}Co_{0.33}Se$//RGO	6 M KOH	0-1.5 V	36.7	750	90.8% (2000 cycles)	11

NiSe-G//AC	6 M KOH	0-1.6 V	50.1	816	84.4% (3000 cycles)	12
$Ni_{0.85}Se$ nanoarray//AC	3 M KOH	0-1.6 V	65.02	103.33	93.7% (10 000 cycles)	13
NiCoP nanoplates//graphene	1 M KOH	0-1.5 V	32.9	1301	83% (5000 cycles)	14
$CoMoO_4$//AC	2M KOH	0-1.8	21.1	300	87.42% (10 000 cycles)	15

Notes and references

1. G. Nagaraju, S. M. Cha, S. C. Sekhar, J. S. Yu, *Adv. Energy Mater.,* 2017**, 7**, 1601362.

2. L. Hou, Y. Shi, C. Wu, Y. Zhang, Y. Ma, X. Sun, J. Sun, X. Zhang, C. Yuan, *Adv. Funct. Mater.,* 2018**, 28**, 1705921.

3. P. Yang, Z. Wu, Y. Jiang, Z. Pan, W. Tian, L. Jiang, L. Hu, *Adv. Energy Mater.,* 2018, **8**, 1801392.

4. C. Xia, Q. Jiang, C. Zhao, P. M. Beaujuge, H. N. Alshareef, *Nano Energy.,* 2016, **24,** 78.

5. J. Huang, J. Wei, Y. Xiao, Y. Xu, Y. Xiao, Y. Wang, L. Tan, K. Yuan, Y. Chen, *ACS Nano,* 2018, **12,** 3030.

6. X. Xiong, G. Waller, D. Ding, D. Chen, B. Rainwater, B. Zhao, Z. Wang, M. Liu, *Nano Energy,* 2015, **16,** 71.

7. J. Yang, C. Yu, X. Fan, S. Liang, S. Li, H. Huang, Z. Ling, C. Hao, J. Qiu, *Energy Environ. Sci.,* 2016, **9,** 1299.

8. L. Shen, L. Yu, H. B. Wu, X.-Y. Yu, X. Zhang, X. W. D. Lou, *Nat. Commun.,* 2015, **6,** 6694.

9. L. Shen, J. Wang, G. Xu, H. Li, H. Dou, X. Zhang, *Adv. Energy Mater.,* 2015, **5,** 1400977.

10. X. Shi, J. Key, S. Ji, V. Linkov, F. Liu, H. Wang, H. Gai, R. Wang, *Small,* 2018, 1802861.

11. H. Chen, S. Chen, M. Fan, C. Li, D. Chen, G. Tian, K. Shu, *J. Mater. Chem. A,* 2015, **3,** 23653.

12. B. Kirubasankar, V. Murugadoss, J. Lin, T. Ding, M. Dong, H. Liu, J. Zhang, T. Li, N. Wang, Z. Guo, *Nanoscale,* 2018, **10,** 20414.

13. L. Du, W. Du, H. Ren, N. Wang, Z. Yao, X. Shi, B. Zhang, J. Zai, X. Qian, *J. Mater. Chem. A,* 2017, **5,** 22527.

14. H. Liang, C. Xia, Q. Jiang, A. N. Gandi, U. Schwingenschlögl, H. N. Alshareef, *Nano Energy,* 2017, **35,** 331.

15. X. Yu, B. Lu, Z. Xu, *Adv. Mater.,* 2014, **26,** 1044.